Motion-Driven Electrochromic Reactions for Self-Powered Smart Window System

Min-Hsin Yeh,[†,‡] Long Lin,[†,‡] Po-Kang Yang,[†] and Zhong Lin Wang*[,†,§]

[†]School of Material Science, Engineering, Georgia Institute of Technology, Atlanta, Georgia 30332-0245, United States and [§]Beijing Institute of Nanoenergy and Nanosystems, Chinese Academy of Sciences, Beijing, China. [‡]M.-H. Yeh and L. Lin contributed equally to this work.

ABSTRACT

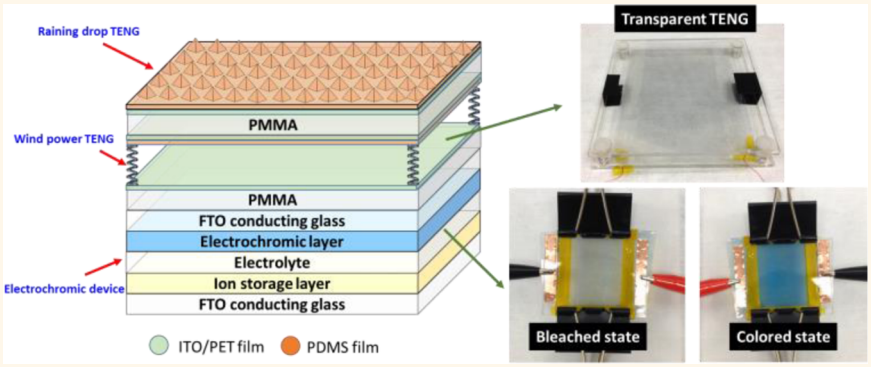

The self-powered system is a promising concept for wireless networks due to its independent and sustainable operations without an external power source. To realize this idea, the triboelectric nanogenerator (TENG) was recently invented, which can effectively convert ambient mechanical energy into electricity to power up portable electronics. In this work, a self-powered smart window system was realized through integrating an electrochromic device (ECD) with a transparent TENG driven by blowing wind and raindrops. Driven by the sustainable output of the TENG, the optical properties, especially the transmittance of the ECD, display reversible variations due to electrochemical redox reactions. The maximum transmittance change at 695 nm can be reached up to 32.4%, which is comparable to that operated by a conventional electrochemical potentiostat (32.6%). This research is a substantial advancement toward the practical application of nanogenerators and self-powered systems.

KEYWORDS: energy harvesting · electrochromic devices · self-powered systems · triboelectric nanogenerators · smart windows

Self-powered systems have been developed to integrate variable devices into a standalone system with multiple functions, including sensing, communication, computation, *etc.*[1,2] The wireless, miniaturized, and large number of components in the system require a renewable, sustainable, and clean power supply, and energy harvesting from the ambient environment will be a perfect solution for this problem.[3−8] In this regard, the triboelectric nanogenerator (TENG) was recently invented to convert mechanical energy into electricity, based on the coupling effect of contact electrification and electrostatic induction.[9,10] In the past few years, the output performance of the TENG has been improved drastically through advanced structural design and material optimization.[11−15] By using nanogenerators as the power source, various types of self-powered systems were successfully demonstrated, such as wireless sensor networks,[16,17] electrochemical reactions,[18,19] chemical sensors,[20] home appliances,[15,21] and security detection.[22] To realize practical and commercial applications of the self-powered system, a fully integrated device with independent working capability is highly desired. Recently, transparent and flexible TENGs have provided a new route to harvest ambient mechanical energy and are more suitable for integration in wearable electronic devices.[23−25]

Electrochromic devices (ECDs) are developed to provide reversible changes of their

* Address correspondence to zhong.wang@mse.gatech.edu.

Received for review January 31, 2015 and accepted March 25, 2015.

Published online March 25, 2015
10.1021/acsnano.5b00706

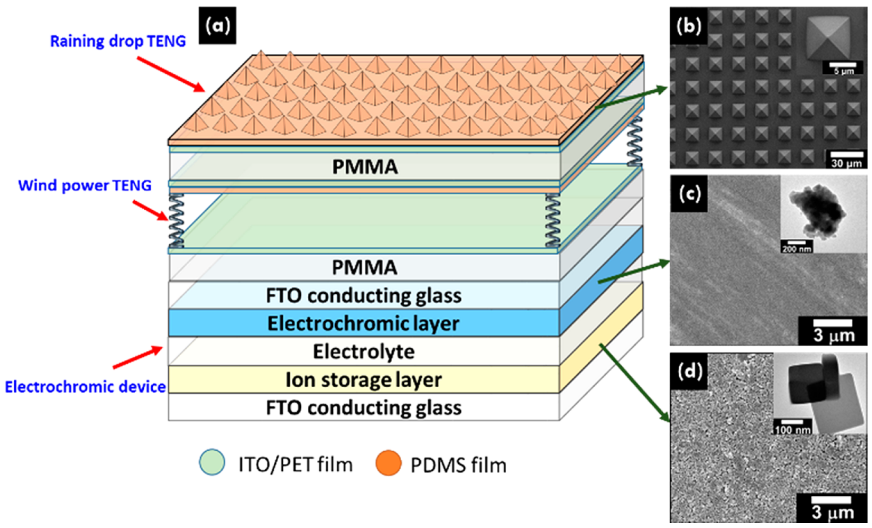

Figure 1. (a) Schematic diagram of the detailed structure of the self-powered smart window integrated with a raindrop-TENG, a wind-powered-TENG, and an ECD from top to bottom. SEM images of (b) the PDMS film with a well-organized micropyramid array structure and (c) the PB and (d) the ZnHCF films. TEM images of PB nanoparticles and ZnHCF nanocubes are also presented as the insets.

optical properties *via* the electrochemical redox reactions corresponding to an external electric field,[26−28] which are widely applied in displays,[29] switchable mirrors,[30] and electronic papers.[31] Specifically, some types of ECDs with a nonvolatile memory effect are ideal candidates for energy-saving smart windows on infrastructures and automobiles, since this type of ECD can maintain a certain coloring state with no additional power supply.[32] In this regard, the ECD can be integrated with a TENG as the power source instead of using batteries to provide a constant voltage across the device as a self-powered smart window system. The concept of a "self-powered electrochromic window" can also be realized by integration with solar cells as the power sources to drive the electrochromic device.[33−35] However, there are unavoidable drawbacks, such as some part of ECD's surface area will be covered or sacrificed by solar cells or the transparency of the integrated device will be reduced since most of the solar cells are not fully transparent, which may limit its practical applications. Here, we proposed a new structure for a self-powered electrochromic window, which is composed of a transparent TENG to harvest natural mechanical energies to drive the ECD and can completely solve the problems mentioned above.

Here in this work, we established a fully integrated self-powered smart window composed of a dual-mode TENG and an ECD. The entire device was a transparent, multilayered structure, which was compatible with the smart window structure. The ECD was composed of Prussian blue (PB) nanoparticles and zinc hexacyanoferrate (ZnHCF) nanocubes as the electrochromic material and the ion storage layer, respectively. By operating with a conventional electrochemical workstation, a maximum reversible change in transmittance (ΔT) of 32.6% could be achieved with respect to an external dc voltage. The TENG consisted of a multilayered structure with micropatterned polydimethylsiloxane (PDMS) thin films and transparent electrodes, which could be employed for harvesting the kinetic energy from wind impact and water droplets, with an optimized output power of 130 mW/m^2. By assembling the two devices on the same substrate, the self-powered smart window system was successfully realized with a transmittance change of up to 32.4% with visualized color variations as well, which could compete with the results demonstrated by the electrochemical workstation. This work sheds light on motion-driven electrochemical reactions and paves the way for promising applications of TENGs, which will push forward the development of self-powered systems.

RESULTS AND DISCUSSION

The multilayer structure of the self-powered smart window is schematically illustrated in Figure 1a. On the top is a single-electrode TENG for scavenging the raindrop kinetic energy that is composed of a PDMS thin film attached to a conducting substrate. A micropatterned pyramid array structure (Figure 1b) was created on the surface of the PDMS thin film through photolithography and a template molding process, which plays an important role in improving the hydrophobic property and effective contact area of the surface, both aiming at enhancing the output performance of the single-electrode TENG. Other types of nanostructures, such as nanodots, nanogrates, and nanomeshes, can also provide a similar function to enhance its performance.[36] With a similar material system, a contact-mode TENG assembled by elastic springs was implemented right beneath the above-mentioned single-electrode-mode TENG. This structure was excellent for harvesting energy from wind

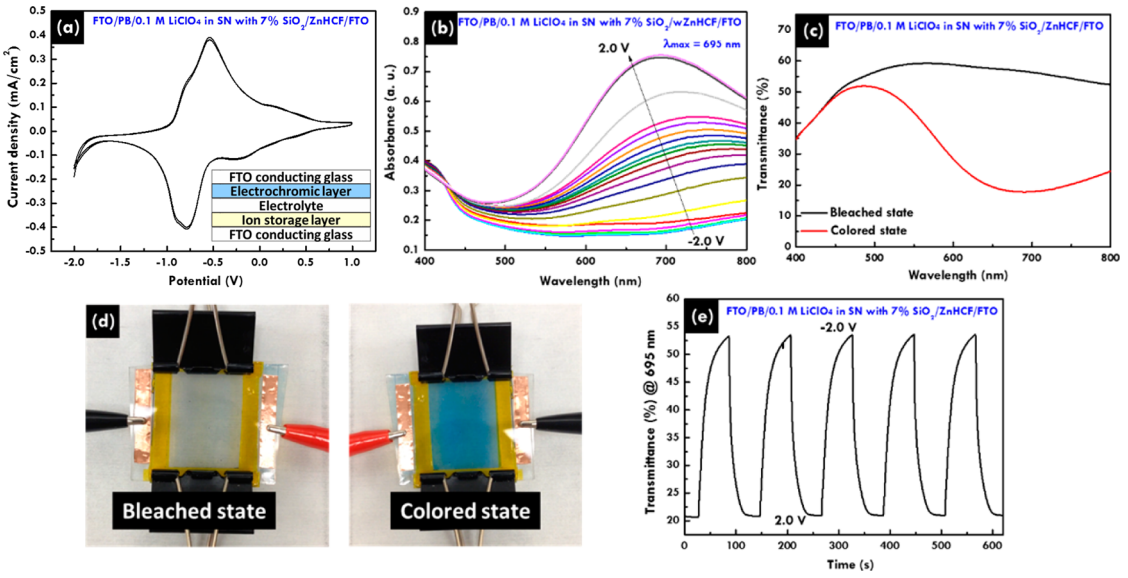

Figure 2. (a) Cyclic voltammogram of the PB/ZnHCF ECD with a SN electrolyte with 0.1 M $LiClO_4$ and 7% SiO_2 under a scan rate of 100 mV/s, obtained between −2.0 and 1.0 V. (b) UV-absorption spectra of the PB/ZnHCF ECD, obtained at different applied potentials from −2.0 to 2.0 V. (c) Transmittance spectra and (d) photographs of the PB/ZnHCF ECD in bleached and colored states, depicting the color change of the ECD from colorless to dark blue at an applied potential from −2.0 to 2.0 V, respectively. (e) Transmittance change of the PB/ZnHCF ECD in repose to changing the potential between −2.0 and 2.0 V at 695 nm.

impact, since the low-elastic-modulus springs could buffer the wind impact and brought the device back to its original shape when the wind stopped. Both the TENGs were stacked on the ECD with a common acrylic substrate to form a fully integrated self-powered system.

For the ECD, water-dispersible PB nanoparticles and ZnHCF nanocubes were synthesized as electrochromic and ion storage materials, respectively (see Experimental Section for details). The phase compositions of the as-synthesized powders were confirmed by X-ray diffraction (Figure S1), and the peaks for each of the XRD patterns canbe assigned to $Fe_4[Fe(CN)_6]_3 \cdot xH_2O$ (JCPDS, PDF no.73-0687)[37] and $Zn_3[Fe(CN)_6]_2$ (JCPDS, PDF no. 38-0688),[38] suggesting that both compounds were successfully synthesized and the residual reagents were completely removed. Uniform PB and ZnHCF films were successfully prepared by spin coating the corresponding dispersions on the FTO conducting glass, as shown in the SEM images (Figure 1c and d). Moreover, the morphologies of PB and ZnHCF powders were characterized by TEM (inset of Figure 1c and d), in which the particle-like PB and cubic-like ZnHCF can be clearly observed. PB-coated and ZnHCF-coated FTO conducting glasses were employed as the working and counter electrode, respectively. The ECD was assembled by sandwiching the solid-state electrolyte (0.1 M $LiClO_4$/SN with 7% SiO_2) between the PB and ZnHCF films.

Before the concurrent operations of the self-powered device, the characterization of each device was carried out individually to evaluate its performance. First, the electrochemical property and electrochromic performance of the ECD were characterized by a conventional electrochemical workstation. Figure 2a shows the cyclic voltammetry analysis of the ECD at a scanning rate of 100 mV/s. One obvious redox peaks around −0.75 V was observed, corresponding to the following reversible redox reaction for the coloring and bleaching process, as shown in eq 1:

$$\underset{\text{(PrussianBlue, darkblue)}}{Fe_4^{III}[Fe^{II}(CN)_6]_3} + 2Li_2Zn^{II}{}_3[Fe^{II}(CN)_6]_2 \underset{\text{(colorless)}}{} \leftrightarrows \underset{\text{(PrussianWhite, colorless)}}{Li_4Fe_4^{II}[Fe^{II}(CN)_6]_3} + 2Zn^{II}{}_3[Fe^{III}(CN)_6]_2 \quad (1)$$

In this reversible reaction, the color change is mainly contributed by the PB electrode. In order to decrease the switching time between the bleached and colored state, a broader potential range between −2.0 and 2.0 V was applied with the consideration of the device stability and the maximum optical attenuation. The electrochromic property of the PB/ZnHCF ECD under various applied potentials was measured by the UV−vis spectrum (Figure 2b). As the voltage across the ECD reached −2.0 V, the absorbance spectrum is mostly referred to as the pristine FTO conducting glass. As the potential difference increases to 2.0 V, a visible absorbance peak at 695 nm can be obtained, which is mainly contributed by the color change of the PB nanoparticles. To obtain a more intuitive view of the change of the optical property, the transmittance of the ECD was measured from 400 to 800 nm both before and after the coloring process, as shown in Figure 2c. It can be found that the transmittance decreased in the full range during the coloring process, and the highest variation was achieved at 695 nm, while the transmittance decreased from 53.5% to 20.9%.

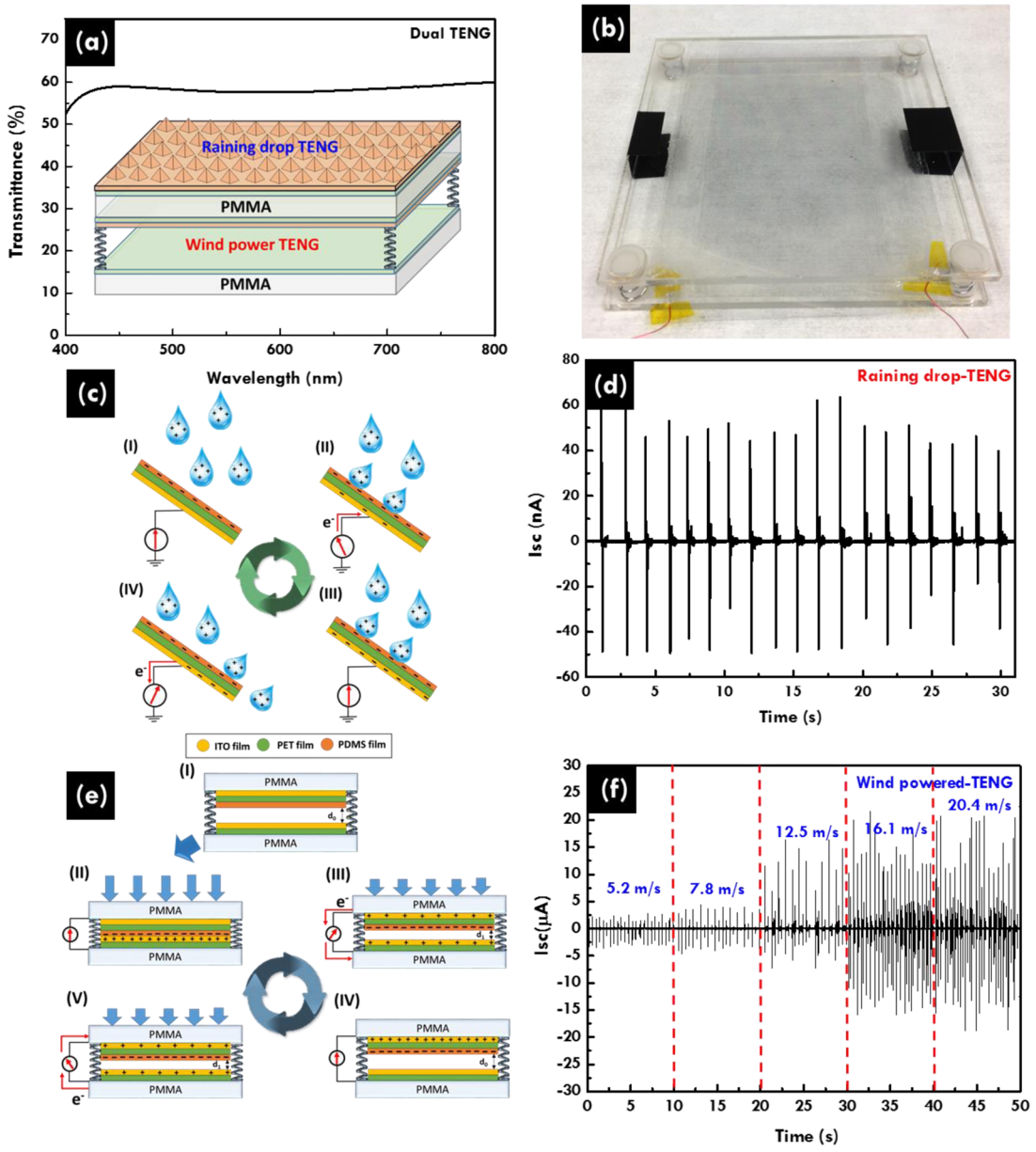

Figure 3. (a) The transmittance spectra of the dual-mode TENG. The schemetic structure of the dual-mode TENG is also shown as the inset. (b) Photograph of the transparent dual-mode TENG. (c) Scheme of the working mechanism of the raindrop-TENG for harvesting falling raindrops' electrostatic energy. (d) Output of the I_{SC} curve of the raindrop-TENG. (e) Scheme of the working mechanism of the wind-powered-TENG for harvesting wind energy. (f) Output of the I_{SC} curve of the wind-powered-TENG with various wind velocities.

This transmittance change can also be observed by visualization, indicating that the appearance of the ECD changed from transparent (bleached state) to deep blue (colored state), as displayed in Figure 2d. The real-time transmittance measurement of the ECD at 695 nm is shown in Figure 2e, by which a stable transmittance change (ΔT) of 32.6% could be verified by multiple cycles of potential scanning from −2.0 to 2.0 V. In addition, the switching times for bleaching (τ_b) and coloring (τ_c) were calculated to be 30 and 20 s, respectively.

On the other hand, the output performances of the dual-mode TENG constituted by a raindrop-TENG and a wind-powered-TENG were also investigated. To accommodate its application in a smart window system, high transparency is an essential factor of the dual-mode TENG, which was obtained by all-transparent materials and was revealed by the transmittance measurement in Figure 3a. Its high tranmittance of over 60% in most of the wavelength range guarantees its compatibility in the smart window system, which is also confirmed by the photograph of the transparent TENG in Figure 3b.

The working mechanism of the dual-mode TENG is based on the coupling of contact electrification and electrostatic induction, which can be explained in two separate parts, as illustrated in Figure 3c and e,

respectively. A single-electrode working mode was applied for harvesting falling raindrop energy,[39] and the flowing of water droplets on the surface of PDMS induces a change in the potential difference and the corresponding charge flow between its bottom electrode and the ground, as indicated in Figure 3c. When the positively charged raindrops[40] contact the hydrophobic PDMS layer with micropyramid structures on its surface (ii), a positive electric potential difference will be induced between the bottom electrode and the ground, which drives the electron flow from the ground to the electrode to balance the electric field (iii). Once the charged raindrops are ejected away from the surface of the hydrophobic PDMS layer, the potential of the ITO electrode will be lower than that of the ground, which means the electrons will flow back in the opposite direction (iv) until the original state (i) is attained. To measure the electric output performance of the raindrop-TENG, tap water was used to simulate raindrops and sprayed on the PDMS surface, and the short-circuit current (I_{SC}) of the raindrop-TENG was recorded and is shown in Figure 3d. The I_{SC} value of the raindrop-TENG is *ca.* 50 nA. This result indicates that raindrop energy generated from the natural environment can be easily harvested by the raindrop-TENG.

Alternatively, a contact-mode TENG was used for harvesting the wind energy.[41] As shown in Figure 3e, the original separation distance (d_0) between the two triboelectric surfaces (*i.e.*, ITO and PDMS) is determined by the elastic constant of the springs and the loading mass (i). The impact from the wind or other mechanical sources will bring the ITO and PDMS layers into full contact. Upon contact, electrons in the ITO layer are transferred into the PDMS layer due to their diverse triboelectric polarities,[42] which results in net negative charges on the PDMS surface and net positive charges on the ITO surface (ii). Once the wind impact stops, the contacting surfaces start to separate due to the restoring force of the springs, and the separation of the triboelectric charges will induce a potential difference between the top and bottom electrodes. In the meantime, the electric potential difference between the ITO and the PDMS layer drives electrons from the outer circuit to screen the positive triboelectric charges on the PDMS layer (iii). When the two triboelectric surfaces move back to the original position, another phase of electric equilibrium will be reached since negative triboelectric charges on the PDMS layer are screened completely, which leaves an equal amount of induced charges on the top ITO layer (iv). Once another gust of wind impacts the surface of the top electrode to reduce the separation distance (d_1), a change of electric potential difference with reversed polarity would be generated and electron flow is further induced through the reverse direction (v). Another equilibrium state would be established after both electrodes reach full contact with each other (ii). This cyclic process corresponds to instantaneously negative and positive induced currents from the wind-powered-TENG. For measuring the electric output performance of the wind-powered-TENG, a compressed air outlet was used to simulate the wind impact. It can be clearly observed that the peak I_{SC} increases with the elevation of wind speed, which indicates that the dynamic current flow is determined by the deformation rate of the TENG (Figure 3f). The maximum I_{SC} value can reach 15 μA with a wind velocity of around 16.1 m/s. This result indicates that the wind energy generated from the natural environment can be easily harvested by the wind-powered-TENG, and the output signal can be utilized for monitoring the ambient wind speed. Moreover, a robust test of the wind-powered-TENG was also performed to investigate its long-term stability. Figure S2 shows that the output performance of the wind-powered-TENG has only a little decay after continuous impacting of 100 000 cycles, indicating that sustainable harvesting of the ambient mechanical energies can be realized *via* this type of TENG with long-term stability.

After characterizing each individual unit of the self-powered smart window system, the electrochromic performance of the integrated ECD driven by the dual-mode TENG was investigated, as shown in Figure 4a. For simplicity purposes, only the wind-powered-TENG was involved in the powering of the smart window, and the implementation of the water-drop-TENG will add to the output current and enhance the overall performance of the integrated device. In addition, a mechanical shaker was used to simulate the wind impact at a constant frequency of 5 Hz. The intensity of the motor impact was set as 28.5 kgf/m^2, which was equivalent to a wind velocity of 16.1 m/s. Moreover, a full-wave bridge rectifier was employed to convert the generated alternating-current (ac) pulses into direct-current (dc) signals, as shown in Figure 4b, and the rectified dc current could generate 140 nC of charge transfer per cycle for driving the ECD. The I_{SC} (*ca.* 45 μA) and the V_{OC} (*ca.* 140 V) of the dual-mode TENG are shown in Figure S3a and b, respectively. The effective output power of the TENG was evaluated by monitoring the voltage and current across variable load resistances ranging from 10 Ω to 1 GΩ (Figure 4c), and an optimized power density of 130 mW/m^2 can be achieved with a load resistance of 4 MΩ (Figure 4d). Figure 4e shows the UV/vis-absorbance change of the self-powered ECD driven by the shaker with various durations from 0 to 5000 s. Significant absorbance differences can be monitored by UV/vis spectroscopy, and photographs of the ECD at various durations are also presented as insets in Figure 4e, showing the color switching of the ECD between colorless and dark blue driven by environmentally induced mechanical motions. Figure 4f shows the transmittance change of the self-powered ECD at a certain wavelength (695 nm) for bleaching and coloring driven by a dual-mode TENG. These results provide solid evidence to support that the self-powered smart window is

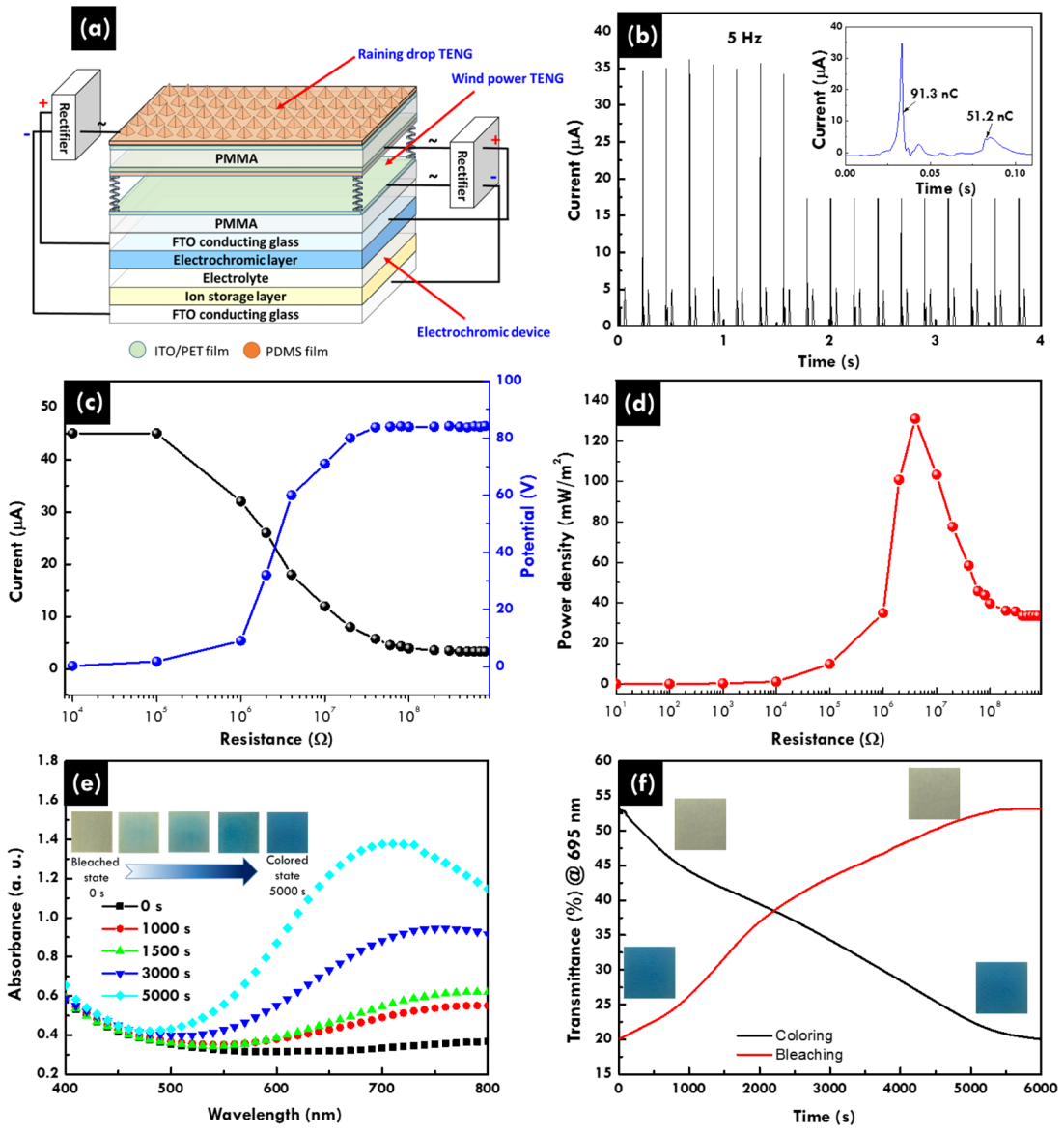

Figure 4. (a) Schematic diagram of the detailed structure of the self-powered smart window integrated with full-wave bridge rectifiers. (b) Output of the rectified I_{SC} curve of the dual-mode TENG. Enlarged views of a single current peak and related current charge are also shown as insets. (c) Dependences of I_{load} and V_{load} of the dual-mode TENG at various load resistances ranging from 10 Ω to 1 GΩ. (d) Instantaneous P of the dual-mode TENG on the resistance of the external load. (e) UV-absorption spectra of the self-powered ECD obtained at different duration times. Pictures of ECD at different duration times are also presented as insets for depicting the changed colors of the ECD at different times. (f) Transmittance change of the self-powered smart window in response to various duration times for bleaching and coloring.

successfully realized by an integrated device with an ECD and a TENG.

To illustrate the working of the self-powered smart window as an integrated device, a series of schematics indicating the coupling of charge transfer and electrochemical reactions in various steps are presented in Figure 5. Since the power generation process of the dual-mode TENG was alreday described in Figure 3, it will not be further discussed here. In the ideal case, the amount of charges injected into the PB layer of a ECD should be equal to the total amount of charge transfer from the two output terminals of the TENG. Here, as depicted in stages (iii) and (v), both the wind-powered- and raindrop-TENGs generate an ac output current with distinct directions of charge flow during a full operation cycle. The direction of the current flow will be regulated by the full-wave bridge rectifier to ensure that the current flow through the ECD will be in a constant direction for charging the PB layer. The charging cycle from stage (ii) to (v) in Figure 5 will keep taking place for harvseting energy and then charging the ECD when the self-powered window system is subject to a continuous wind impact or falling raindrops.

CONCLUSIONS

In summary, the concept of a motion-driven self-powered smart window system was realized by

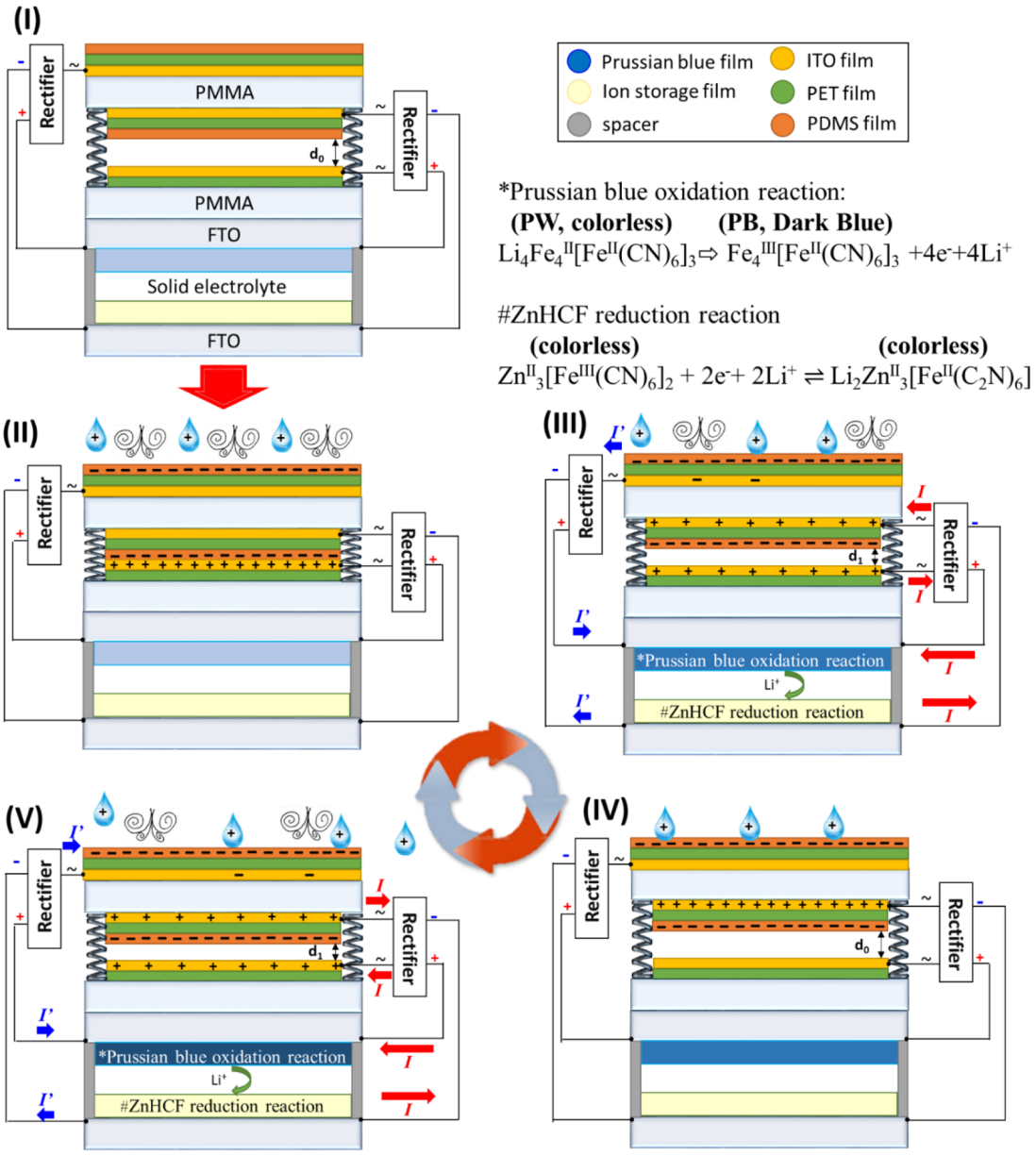

Figure 5. Scheme of the working mechanism of the self-powered window for spontaneously harvesting falling raindrops' electrostatic energy and wind energy.

integrating an electrochromic device with a dual-mode triboelectric nanogenerator. The TENG can take advantage of environmental oscillations such as blowing wind and raindrops to deliver an output current of up to 45 μA, corresponding to an effective power density of 130 mW/m^2. Reversible electrochromic reactions can be driven directly by the TENG, and a maximum transmittance change of 32.4% as well as visible color change can be obtained, which is comparable to the ECD driven by an electrochemical workstation. This research presents a substantial advancement in the practical applications of nanogenrators and self-powered systems, which will initiate promissing improvements in self-powered flexible displays, wearable electronics, and energy efficient buildings.

METHODS

Synthesis of Water-Dispersible Prussian Blue Nanoparticles and Zinc Hexacyanoferrate Nanocubes. The method for synthesizing water-dispersible ferric hexacyanoferrate ($Fe_4[Fe(CN)_6]_3 \cdot xH_2O$), Prussian blue (PB), nanoparticles is based on the modified procedure proposed by Gotoh *et al.*[43] Briefly, 30 mL of an $Fe(NO_3)_3 \cdot 9H_2O$ aqueous solution (0.67 M) was added to 60 mL of a $K_4[Fe(CN)_6] \cdot 3H_2O$ aqueous solution (0.25 M). The blue precipitate was vigorously shaken for 15 min and then rinsed with DI-water six times. After that, an aqueous $K_4[Fe(CN)_6] \cdot 3H_2O$ solution was again added to the blue precipitate with vigorous stirring for 1 week and then dried under reduced pressure to obtain the

water-dispersible PB nanoparticles. On the other hand, zinc hexacyanoferrate (ZnHCF, $Zn_3[Fe(CN)_6]_2$) nanocubes were prepared by a process similar to that mentioned above. Concisely, 30 mL of a $Zn(NO3)_2 \cdot 6H_2O$ aqueous solution (1.33 M) was mixed with 60 mL of a $K_4[Fe(CN)_6] \cdot 3H_2O$ aqueous solution (0.22 M), and a white precipitate was attained. After using DI-water to rinse the sample several times, the ZnHCF solution was further added to the $K_4[Fe(CN)_6] \cdot 3H_2O$ solution under vigorous stirring for 3 days. Water-dispersible ZnHCF nanocubes were obtained after removing the solvent through a vacuum-drying procedure.

Assembly and Characterization of Electrochromic Devices. Water-dispersible PB and ZnHCF inks were separately prepared by introducing 0.1 g of each powder into 1 mL of DI-water. Well-dispersed inks were obtained after vigorous stirring. PB and ZnHCF films were prepared by spin coating the corresponding inks on FTO conducting glasses under 1500 rpm for 10 s. The active area of each spin-coated electrode was controlled to be 2.0 × 3.0 cm^2. Prepared electrodes were stored at room temperature before assembly and characterization. The ECD was assembled by two pieces of FTO conducting glasses that were separately coated with PB and ZnHCF films as the working electrode and the counter electrode, respectively. For preparing the solid-state electrolyte, 0.1 g of $LiClO_4$ was added to 10 mL of liquefied SN at 70 °C, and the solution was then vigorously stirred for 30 min. SiO_2 NPs (7 wt %) were then added to the matrix to eliminate the crystalline structure of SN. Last, a 0.1 M $LiClO_4$/SN solution containing 7 wt % SiO_2 NPs was used as the solid-state electrolyte and sealed between the two electrodes separated by a Kapton spacer tape.

Fabrication Process of the Self-Powered Smart Window. The self-powered smart window is a fully integrated device constituted by a raindrop-TENG, a wind-powered-TENG, and an ECD, as shown in Figure 1a. On the top of the integrated device, the raindrop-TENG, which was built up by ITO/PET with a hydrophobic PDMS film containing a micropyramid array structure, acted as the output 1 of the dual-mode TENG for harvesting the water drop energy. The detailed procedures for preparing the PDMS film with a micropyramid array structure are described in the Supporting Information. On the other hand, the wind-powered-TENG was fabricated by a layered structure with two PMMA substrates. The PDMS-coated ITO/PET and the pristine ITO/PET acting as electrodes were attached on the surface of the PMMA substrates. The two PMMA substrates were separated by four elastic springs at the corners to form spacing between the ITO and the PDMS. This is output 2 of the dual-mode TENG for harvesting wind energy. After that, the raindrop-TENG and ECD can be easily integrated on the top and bottom of the wind-powered-TENG to make a self-powered smart window, respectively.

Characterization. PB and ZnHCF powders were characterized by X-ray diffraction patterns (XRD, Ultima IV, Rigaku) with Cu Kα radiation with 2θ scanning from 10° to 80° at a scan rate of 10 deg min^{-1} to verify their phase compositions. The particle size and geometric nanostructure of PB and ZnHCF powders were characterized by transmission electron microscopy (TEM, JEM-1230, JEOL). The surface morphologies of PB and ZnHCF films were examined by scanning electron microscopy (SEM, Nova NanoSEM 230, FEI). The surface morphology of the PDMS film containing a micropyramid array structure was also shown by field emission scanning electron microscopy (FE-SEM, SU8010, Hitachi). Electrochemical characterization of ECDs was measured and recorded through an electrochemical potentiostat (model VersaSTAT 3, Princeton Applied Research). All optical properties were obtained *via* a UV−vis spectrophotometer (V630, Jasco). In the electric output measurement of the raindrop-TENG and wind-powered-TENG, a programmable electrometer (model 6514, Keithley) and a low-noise current preamplifier (model SR570, Stanford Research System) were used for recording the output voltage and current, respectively. Moreover, in order to simulate the condition of continuously blowing winds, a mechanical shaker (Labworks SC121) was used to drive the wind-powered-TENG for periodical contacting and separating.

Conflict of Interest: The authors declare no competing financial interest.

Supporting Information Available: Materials, related characterization of materials, and performance of TENG devices are provided in the Supporting Information. This material is available free of charge *via* the Internet at http://pubs.acs.org.

Acknowledgment. This work was supported by the U.S. Department of Energy, Office of Basic Energy Sciences (DE-FG02-07ER46394), the Hightower Chair Foundation, and the "Thousands Talents" program for pioneer researcher and his innovation team, China. M.H.Y. thanks the support from Ministry of Science and Technology, Taiwan (MOST 103-2917-I-564-070).

REFERENCES AND NOTES

1. Wang, Z. L. Self-Powered Nanotech. *Sci. Am.* **2008**, *298*, 82–87.
2. Beeby, S. P.; Tudor, M. J.; White, N. M. Energy Harvesting Vibration Sources for Microsystems Applications. *Meas. Sci. Technol.* **2006**, *17*, R175–R195.
3. Dresselhaus, M. S.; Thomas, I. L. Alternative Energy Technologies. *Nature* **2001**, *414*, 332–337.
4. O'Regan, B.; Grätzel, M. A Low-Cost, High-Efficiency Solar Cell Based on Dye-Sensitized Colloidal TiO_2 Films. *Nature* **1991**, *353*, 737–740.
5. Wang, Z. L.; Song, J. Piezoelectric Nanogenerators Based on Zinc Oxide Nanowire Arrays. *Science* **2006**, *312*, 242–246.
6. Calabrese Barton, S.; Gallaway, J.; Atanassov, P. Enzymatic Biofuel Cells for Implantable and Microscale Devices. *Chem. Rev.* **2004**, *104*, 4867–4886.
7. Tu, W.; Zhou, Y.; Liu, Q.; Tian, Z.; Gao, J.; Chen, X.; Zhang, H.; Liu, J.; Zou, Z. Robust Hollow Spheres Consisting of Alternating Titania Nanosheets and Graphene Nanosheets with High Photocatalytic Activity for CO_2 Conversion into Renewable Fuels. *Adv. Funct. Mater.* **2012**, *22*, 1215–1221.
8. Chen, L.; Zhou, Y.; Dai, H.; Yu, T.; Liu, J.; Zou, Z. One-Step Growth of $CoNi_2S_4$ Nanoribbons on Carbon Fibers as Platinum-Free Counter Electrodes for Fiber-Shaped Dye-Sensitized Solar Cells with High Performance: Polymorph-Dependent Conversion Efficiency. *Nano Energy* **2015**, *11*, 697–703.
9. Fan, F. R.; Tian, Z. Q.; Lin Wang, Z. Flexible Triboelectric Generator. *Nano Energy* **2012**, *1*, 328–334.
10. Wang, Z. L. Triboelectric Nanogenerators as New Energy Technology for Self-Powered Systems and as Active Mechanical and Chemical Sensors. *ACS Nano* **2013**, *7*, 9533–9557.
11. Lin, L.; Wang, S.; Xie, Y.; Jing, Q.; Niu, S.; Hu, Y.; Wang, Z. L. Segmentally Structured Disk Triboelectric Nanogenerator for Harvesting Rotational Mechanical Energy. *Nano Lett.* **2013**, *13*, 2916–2923.
12. Zhu, G.; Bai, P.; Chen, J.; Lin Wang, Z. Power-Generating Shoe Insole Based on Triboelectric Nanogenerators for Self-Powered Consumer Electronics. *Nano Energy* **2013**, *2*, 688–692.
13. Wang, S.; Xie, Y.; Niu, S.; Lin, L.; Liu, C.; Zhou, Y. S.; Wang, Z. L. Maximum Surface Charge Density for Triboelectric Nanogenerators Achieved by Ionized-Air Injection: Methodology and Theoretical Understanding. *Adv. Mater.* **2014**, *26*, 6720–6728.
14. Xie, Y.; Wang, S.; Niu, S.; Lin, L.; Jing, Q.; Su, Y.; Wu, Z.; Wang, Z. L. Multi-Layered Disk Triboelectric Nanogenerator for Harvesting Hydropower. *Nano Energy* **2014**, *6*, 129–136.
15. Zhu, G.; Chen, J.; Zhang, T.; Jing, Q.; Wang, Z. L. Radial-Arrayed Rotary Electrification for High Performance Triboelectric Generator. *Nat. Commun.* **2014**, *5*, 3426.
16. Wang, S.; Lin, L.; Wang, Z. L. Nanoscale Triboelectric-Effect-Enabled Energy Conversion for Sustainably Powering Portable Electronics. *Nano Lett.* **2012**, *12*, 6339–6346.
17. Tang, W.; Meng, B.; Zhang, H. X. Investigation of Power Generation Based on Stacked Triboelectric Nanogenerator. *Nano Energy* **2013**, *2*, 1164–1171.
18. Zhu, G.; Pan, C.; Guo, W.; Chen, C. Y.; Zhou, Y.; Yu, R.; Wang, Z. L. Triboelectric-Generator-Driven Pulse Electrodeposition for Micropatterning. *Nano Lett.* **2012**, *12*, 4960–4965.

19. Yang, X.; Zhu, G.; Wang, S.; Zhang, R.; Lin, L.; Wu, W.; Wang, Z. L. A Self-Powered Electrochromic Device Driven by a Nanogenerator. *Energy Environ. Sci.* **2012**, *5*, 9462–9466.
20. Lin, Z. H.; Zhu, G.; Zhou, Y. S.; Yang, Y.; Bai, P.; Chen, J.; Wang, Z. L. A Self-Powered Triboelectric Nanosensor for Mercury Ion Detection. *Angew. Chem., Int. Ed.* **2013**, *52*, 5065–5069.
21. Zhu, G.; Zhou, Y. S.; Bai, P.; Meng, X. S.; Jing, Q.; Chen, J.; Wang, Z. L. A Shape-Adaptive Thin-Film-Based Approach for 50% High-Efficiency Energy Generation through Micro-Grating Sliding Electrification. *Adv. Mater.* **2014**, *26*, 3788–3796.
22. Zhu, G.; Yang, W. Q.; Zhang, T.; Jing, Q.; Chen, J.; Zhou, Y. S.; Bai, P.; Wang, Z. L. Self-Powered, Ultrasensitive, Flexible Tactile Sensors Based on Contact Electrification. *Nano Lett.* **2014**, *14*, 3208–3213.
23. Kim, S.; Gupta, M. K.; Lee, K. Y.; Sohn, A.; Kim, T. Y.; Shin, K. S.; Kim, D.; Kim, S. K.; Lee, K. H.; Shin, H. J.; *et al*. Transparent Flexible Graphene Triboelectric Nanogenerators. *Adv. Mater.* **2014**, *26*, 3918–3925.
24. Meng, B.; Tang, W.; Too, Z.-h.; Zhang, X.; Han, M.; Liu, W.; Zhang, H. A Transparent Single-Friction-Surface Triboelectric Generator and Self-Powered Touch Sensor. *Energy Environ. Sci.* **2013**, *6*, 3235–3240.
25. Ko, Y. H.; Nagaraju, G.; Lee, S. H.; Yu, J. S. PDMS-Based Triboelectric and Transparent Nanogenerators with ZnO Nanorod Arrays. *ACS Appl. Mater. Interface* **2014**, *6*, 6631–6637.
26. Beaujuge, P. M.; Reynolds, J. R. Color Control in Π-Conjugated Organic Polymers for Use in Electrochromic Devices. *Chem. Rev.* **2010**, *110*, 268–320.
27. Rosseinsky, D. R.; Mortimer, R. J. Electrochromic Systems and the Prospects for Devices. *Adv. Mater.* **2001**, *13*, 783–793.
28. DeLongchamp, D. M.; Kastantin, M.; Hammond, P. T. High-Contrast Electrochromism from Layer-by-Layer Polymer Films. *Chem. Mater.* **2003**, *15*, 1575–1586.
29. Mortimer, R. J.; Dyer, A. L.; Reynolds, J. R. Electrochromic Organic and Polymeric Materials for Display Applications. *Displays* **2006**, *27*, 2–18.
30. Richardson, T. New Electrochromic Mirror Systems. *Solid State Ionics* **2003**, *165*, 305–308.
31. Andersson, P.; Nilsson, D.; Svensson, P. O.; Chen, M.; Malmström, A.; Remonen, T.; Kugler, T.; Berggren, M. Active Matrix Displays Based on All-Organic Electrochemical Smart Pixels Printed on Paper. *Adv. Mater.* **2002**, *14*, 1460–1464.
32. Su, L.; Wang, H.; Lu, Z. All-Solid-State Electrochromic Window of Prussian Blue and Electrodeposited WO_3 Film with Poly(ethylene oxide) Gel Electrolyte. *Mater. Chem. Phys.* **1998**, *56*, 266–270.
33. Hsu, C. Y.; Lee, K. M.; Huang, J. H.; Justin Thomas, K. R.; Lin, J. T.; Ho, K. C. A Novel Photoelectrochromic Device with Dual Application Based on Poly(3,4-alkylenedioxythiophene) Thin Film and an Organic Dye. *J. Power Sources* **2008**, *185*, 1505–1508.
34. Xie, Z.; Jin, X.; Chen, G.; Xu, J.; Chen, D.; Shen, G. Integrated Smart Electrochromic Windows for Energy Saving and Storage Applications. *Chem. Commun.* **2014**, *50*, 608–10.
35. Dyer, A. L.; Bulloch, R. H.; Zhou, Y.; Kippelen, B.; Reynolds, J. R.; Zhang, F. A Vertically Integrated Solar-Powered Electrochromic Window for Energy Efficient Buildings. *Adv. Mater.* **2014**, *26*, 4895–4900.
36. Jeong, C. K.; Baek, K. M.; Niu, S.; Nam, T. W.; Hur, Y. H.; Park, D. Y.; Hwang, G. T.; Byun, M.; Wang, Z. L.; Jung, Y. S.; *et al*. Topographically-Designed Triboelectric Nanogenerator via Block Copolymer Self-Assembly. *Nano Lett.* **2014**, *14*, 7031–7038.
37. Lee, S. H.; Huh, Y. D. Preferential Evolution of Prussian Blue's Morphology from Cube to Hexapod. *Bull. Korean Chem. Soc.* **2012**, *33*, 1078–1080.
38. Kao, S. Y.; Lin, Y. S.; Chin, K.; Hu, C. W.; Leung, M. k.; Ho, K. C. High Contrast and Low-Driving Voltage Electrochromic Device Containing Triphenylamine Dendritic Polymer and Zinc Hexacyanoferrate. *Sol. Energy Mater. Sol. Cells* **2014**, *125*, 261–267.
39. Yang, Y.; Zhang, H.; Chen, J.; Jing, Q.; Zhou, Y. S.; Wen, X.; Wang, Z. L. Single-Electrode-Based Sliding Triboelectric Nanogenerator for Self-Powered Displacement Vector Sensor System. *ACS Nano* **2013**, *7*, 7342–7351.
40. Lin, Z. H.; Cheng, G.; Wu, W.; Pradel, K. C.; Wang, Z. L. Dual-Mode Triboelectric Nanogenerator for Harvesting Water Energy and as a Self-Powered Ethanol Nanosensor. *ACS Nano* **2014**, *8*, 6440–6448.
41. Zhu, G.; Lin, Z. H.; Jing, Q.; Bai, P.; Pan, C.; Yang, Y.; Zhou, Y.; Wang, Z. L. Toward Large-Scale Energy Harvesting by a Nanoparticle-Enhanced Triboelectric Nanogenerator. *Nano Lett.* **2013**, *13*, 847–853.
42. Fan, F. R.; Lin, L.; Zhu, G.; Wu, W.; Zhang, R.; Wang, Z. L. Transparent Triboelectric Nanogenerators and Self-Powered Pressure Sensors Based on Micropatterned Plastic Films. *Nano Lett.* **2012**, *12*, 3109–3114.
43. Gotoh, A.; Uchida, H.; Ishizaki, M.; Satoh, T.; Kaga, S.; Okamoto, S.; Ohta, M.; Sakamoto, M.; Kawamoto, T.; Tanaka, H.; *et al*. Simple Synthesis of Three Primary Colour Nanoparticle Inks of Prussian Blue and Its Analogues. *Nanotechnology* **2007**, *18*, 345609.